
Article:
Zhao, H., Wynne, B.P. orcid.org/0000-0001-6536-7004 and Palmiere, E.J. orcid.org/0000-0002-4048-8536 (2017) Effect of austenite grain size on the bainitic ferrite morphology and grain refinement of a pipeline steel after continuous cooling. Materials Characterization, 123. pp. 128-136. ISSN 1044-5803

https://doi.org/10.1016/j.matchar.2016.11.025

Effect of Austenite Grain Size on the Bainitic Ferrite Morphology and Grain Refinement of a Pipeline Steel after Continuous Cooling

H. Zhao, B.P. Wynne and E.J. Palmiere*

Department of Materials Science and Engineering, The University of Sheffield, Mappin Street, Sheffield S1 3JD, UK

Corresponding author：e.j.palmiere@sheffield.ac.uk

Keywords: Austenite grain size; bainitic ferrite; Bain group; close-packed plane group; grain refinement

Abstract:

The effect of prior-austenite grain size (PAGS) on bainitic ferrite (BF) morphology and effective grain size in a pipeline steel under an industrial cooling conditions was investigated. With PAGSs of 22.3 μm and 37.0 μm, BF laths with a parallel morphology could be seen, while as the PAGS is increased to 52.4 μm or 62.8 μm, more interlocking BF microstructures were observed. Detailed crystallographic analysis identified that intense BF variant selection occurs for the small-grained austenite, but due to the large austenite grain quantity and thus the large total austenite grain boundary area per unit volume of the small-grained austenite, with the reduction

of PAGS from 62.8 μm to 22.3 μm, the effective grain size of the transformed microstructure gradually decreases from 9.5 μm to 5.6 μm. In the meanwhile, the small-grained austenite transformation was dominated by one close-packed plane (CP) group, but for the larger austenite grain, different CP groups were observed to be adjacent to each other, producing the interlocking structure. A mechanism based on the carbon distribution near the BF/austenite interface is proposed to account for this difference.

1. Introduction

Bainitic microstructures have been widely used for enhancing mechanical properties in pipeline steels [1]. Owing to the low carbon concentration in these steels, cementite is usually absent, yielding a non-lamellar microstructure consisting of bainitic ferrite (BF) and micro-constituents such as martensite and retained austenite (M/A). The BF grows in the form of clusters of thin lenticular plates or laths, known as packets and the formation of M/A constituents can be attributed to the partitioning of carbon from these BF laths to the austenite during cooling [2].

The importance of prior-austenite grain size (PAGS) for bainite transformation is well acknowledged. Many investigations [3-6] found that the rate of bainite transformation is increased by decreasing PAGS, which was attributed to an increased austenite grain boundary density, and thus an enhanced nucleation rate. Conversely, other research have shown no appreciable effect of PAGS [7], or a reduction in transformation rate with a smaller PAGS [8, 9]. Additionally, the influence of PAGS

has been suggested not to be continuous, and that there is a critical austenite grain size below which there is a distinct grain size effect [9]. To explain these conflicting observations, Matsuzaki and Bhadeshia [10] identified that different steels can show opposite PAGS effects, and that the discrepancy in kinetic behaviour is accompanied by obvious distinctions between the bainite microstructures. They hypothesised that the overall kinetics of the bainitic transformation is increased by a decrease in PAGS when the overall kinetics is limited by a slow growth rate, whereas the prior-austenite grain refinement reduces the overall kinetics for rapid growth from a limited number of nucleation sites. Furthermore, reducing PAGS has also be shown to lower the bainite-start temperature [5, 11], and a new empirical equation for the bainite-start temperature, considering the effect of both chemical composition and PAGS has recently been developed [11].

Despite the number of studies concerning the effect of PAGS on BF transformation kinetics, there are few investigations regarding the influence of PAGS on BF microstructures and grain refinement. Therefore, in this research specimens with various austenite grain sizes were processed to investigate the effect of PAGS before continuous cooling on the microstructural evolution and grain refinement.

2. Experimental Details

The chemical composition of the tested steel is shown in Table 1. The carbon content of this steel was lowered to 0.045% to improve the weldability, toughness and the solubility of such high concentrations of niobium [12]. Titanium was added to fix

the nitrogen and refine the austenite grain during solidification and subsequent reheating.

Table 1 Chemical Compositions (wt%)

C	Mn	Si	S	P	Nb	Cr	Ni	Cu	Ti	N
0.045	1.43	0.14	<0.003	<0.01	0.09	0.21	0.12	0.21	0.01	0.0039

In order to fully exploit the Nb concentration in this steel, and to fully dissolve its precipitates and shorten the preheating time during testing, all specimens were subjected to solid-solution heat treatments at 1250˚C with argon atmosphere protection, and then were water quenched directly from 1250˚C to room temperature.

The processing route is schematically illustrated in Figure 1. The heat treated specimens were reheated to 1200˚C at a rate of 10˚C/s, held for 2 minutes for equilibration, and then cooled at a rate of 5˚C/s to 1100˚C for a roughing deformation (strain1) at a constant true strain rate of $10s^{-1}$. Following roughing, the specimens were cooled immediately to 950˚C at a rate of 5˚C/s, followed by an accelerated cooling from 950˚C to 500˚C at a rate of 10˚C/s. After that, specimens were slowly cooled from 500˚C to 350˚C at a rate of 1˚C/s and finally water quenched from 350˚C to room temperature.

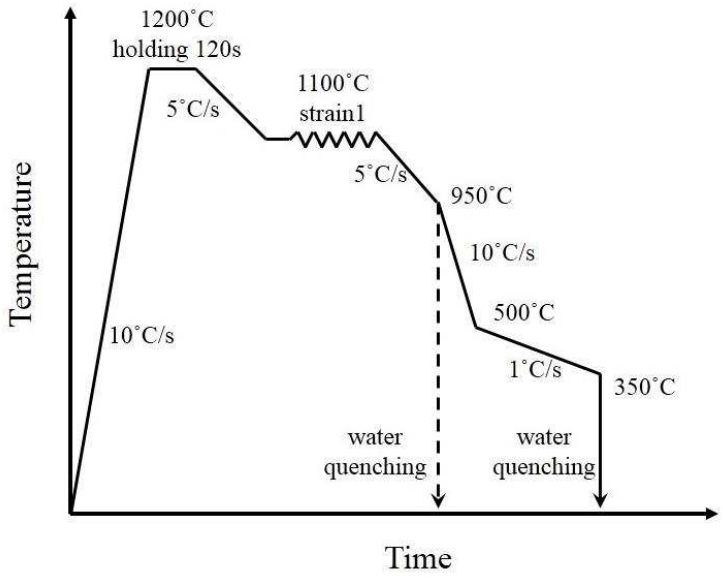

Figure 1 Schematic illustration of the thermomechanical testing profile.

During the solid-solution heat treatment and the thermomechanical processing illustrated above, parameters of the solid-solution heat treatment, the reheating and the roughing deformation (strain1) all can influence the PAGS before the continuous cooling. However, attention must be paid on choosing the suitable parameters to generate different PAGSs, especially the reheating temperature and duration. During reheating, not only the PAGS but also the dissolution status of Nb precipitates are changed by altering the reheating temperatures or durations [13], which makes the investigation on the effect of PAGS biased. Differently, if the standard solid-solution heat treatment can dissolve most of the Nb precipitates, prolonging the duration of the heat treatment can result in a larger PAGS without greatly changing the Nb precipitate dissolution status. In addition, changing the rough deformation (strain1) also has little influence on the Nb precipitate dissolution status simply due to the high temperature (1100˚C) of this deformation at which the solute supersaturation, and subsequently the

extent of precipitation of Nb carbide or carbonitride is very slow. Therefore, to generate austenite with different grain sizes, different parameters of the solid solution heat treatment and the rough deformation (strain 1) were used as shown in Table 2 and S, M, L and XL were designated to the specimens subjected to these different combinations of heat treatment durations and volumes of strain1. Additionally, specimen S, M, L and XL were also water quenched directly from 950˚C before the continuous cooling to reveal the prior-austenite microstructures with different PAGSs.

Table 2 Heat treatment and austenite deformation parameters

Specimen names	S	M	L	XL
Heat treatment temperature (˚C)	1250	1250	1250	1250
Heat treatment duration (s)	1800	1800	7200	7200
Strain1 volume	0.7	0.3	0.3	0
Prior-austenite grain size (μm)	22.3	37.0	52.4	62.8

Samples for metallographic observation were cut on the rolling direction (RD) – normal direction (ND) plane and prepared carefully following standard methods [14]. A 2% nital solution was used to show the transformed microstructure and a saturated aqueous picric acid solution was used to reveal the prior-austenite grain boundaries (PAGBs) [15, 16]. PAGSs were measure optically by the linear intercept method.

EBSD analyses were also carried out via a FEI Sirion electron microscope with an HKL Nordlys detector. EBSD mappings with a step size of 0.2 μm and

accelerating voltage of 20 kV were performed on the RD-ND plane of each sample.

3. Results

3.1 Prior-austenite microstructures

Optical micrographs of the prior-austenite grain boundaries (PAGBs) before the continuous cooling for specimen S, M, L and XL are shown in Figure 2. It is clear from Figure 2 (a)~(d) that through adjusting the solid-solution heat treatment durations and the volumes of strain1, fully recrystallised austenite with different grain sizes were successfully developed before the continuous cooling. PAGS measurement results are shown in Table 2, showing PAGS varying from 22.3 μm to 62.8 μm.

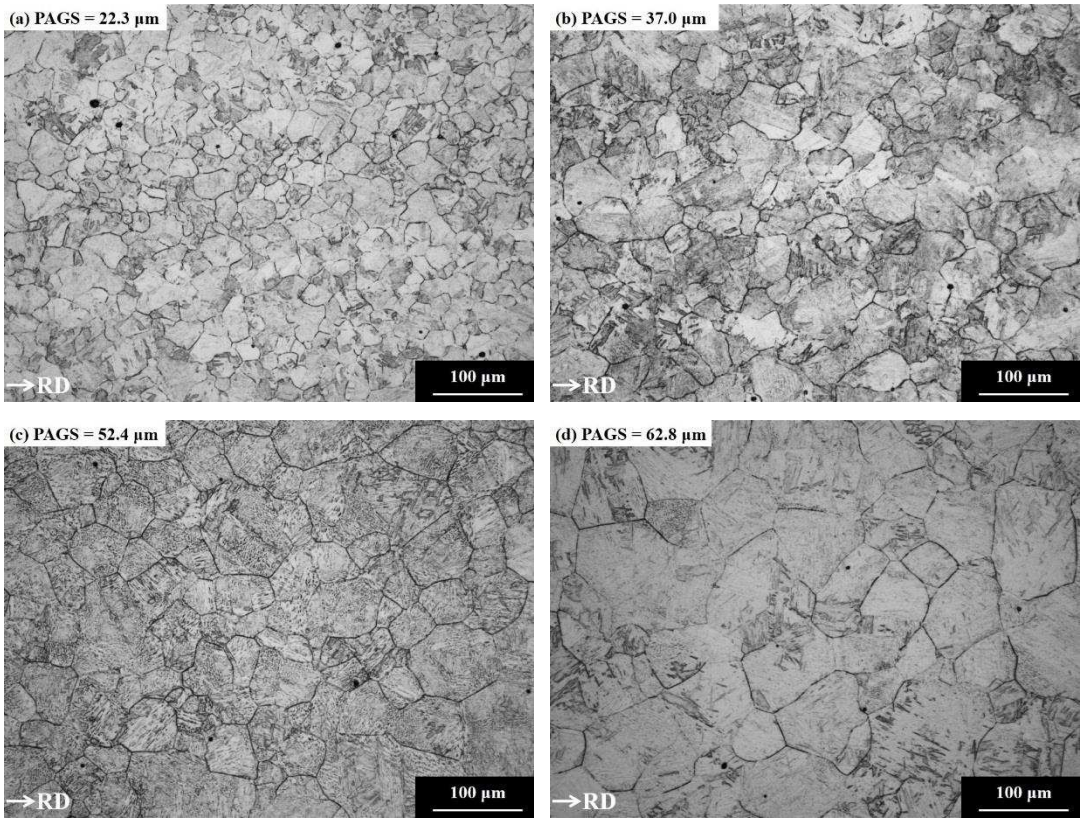

Figure 2 Optical micrographs of the prior-austenite grain boundaries: (a)~(d) for specimen S, M, L and XL respectively.

3.2 Transformed microstructures

Optical micrographs of the continuously cooled microstructures with different PAGSs are shown in Figure 3. The transformed microstructures all consist of BF but with clear differences in their morphologies. With PAGS of 37.0 μm, Figure 3 (b), the transformed microstructure mainly consists of packets of parallel BF laths. With an increased PAGS, Figure 3 (c)~(d), the BF lath boundaries are more and more obscure and irregularly shaped and the shape of the M/A constituents also changes from acicular to equiaxed. Due to the very small PAGS (22.3 μm), the microstructure shown in Figure 3(a) is well refined and the morphology of the BF microstructure can not be observed clearly from this optical micrograph.

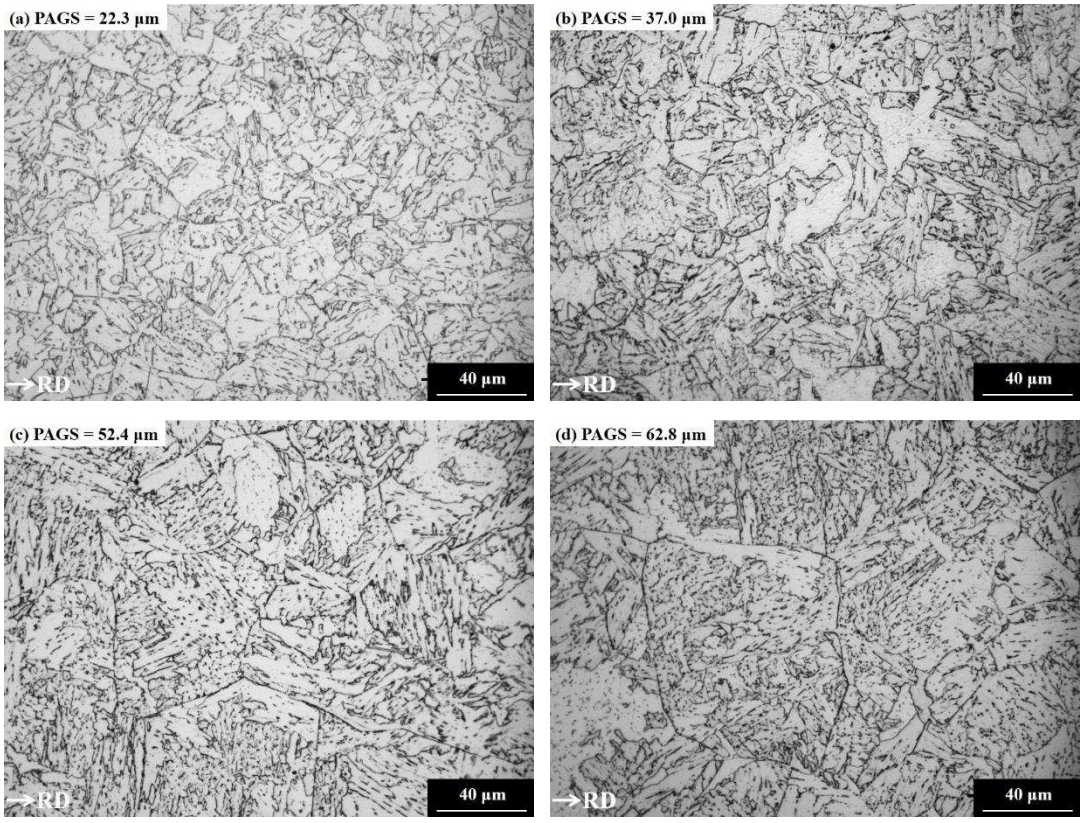

Figure 3 Optical micrographs depicting continuously cooled microstructures with different PAGSs: (a) 22.3 *μm, (b) 37.0 μm, (c) 52.4 μm and (d) 62.8 μm.*

To observe the transformed microstructures in greater detail, SEM secondary electron micrographs of the continuously cooled microstructures with different PAGSs are shown in Figure 4. With PAGSs of 22.3 μm and 37.0 μm, BF laths with a parallel morphology can be observed clearly. However, as the PAGS is increased to 52.4 μm or 62.8 μm, more interlocking BF microstructures are observed in Figure 4 (c)~(d). In these microstructures, BF laths with different directions intersect with each other.

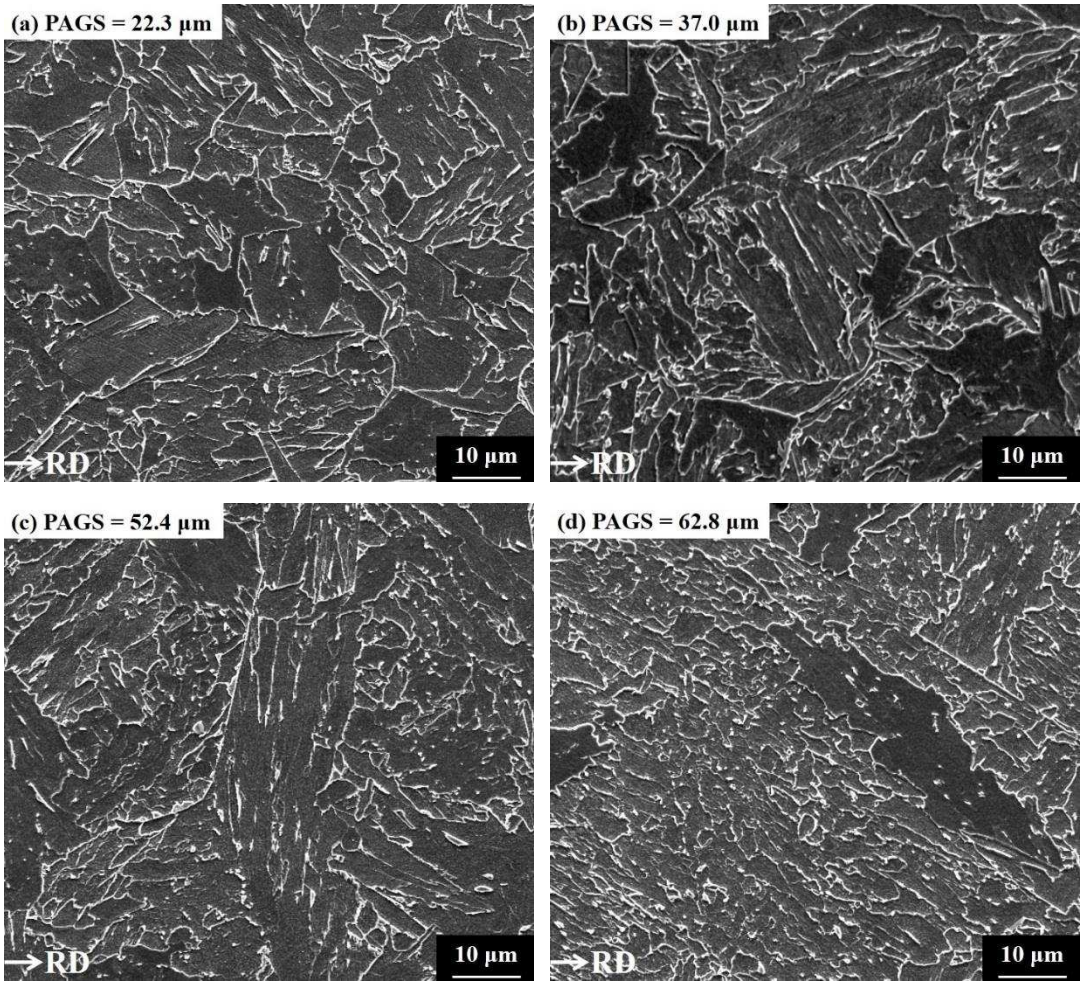

Figure 4 SEM secondary electron micrographs showing the continuously cooled microstructures with different PAGSs: (a) 22.3 *µm, (b) 37.0 µm, (c) 52.4 µm and (d)* 62.8 *µm.*

3.3 EBSD mappings

A small area of each EBSD mapping data set was used to plot an inverse pole figure (IPF) coloured orientation map and a corresponding boundary map. For a statistical analysis of the boundary interception length and boundary density distribution, each whole data set was used.

The selected area IPF coloured orientation maps and corresponding boundary maps of the continuously cooled microstructures with different PAGSs are shown in

Figure 5. It can be seen from Figure 5 that increasing PAGS, the density of high angle grain boundary (HAGB, $\theta \geq 15^{\circ}$) is reduced and the fraction of low angle grain boundary (LAGB, $15^{\circ} > \theta > 3^{\circ}$) is increased, where θ is the boundary disorientation angle. More importantly, as the PAGS is increased, the shape of the LAGB changes from parallel and straight to curved and irregularly arranged, and simultaneously the morphology of the transformed microstructure become increasingly intricate.

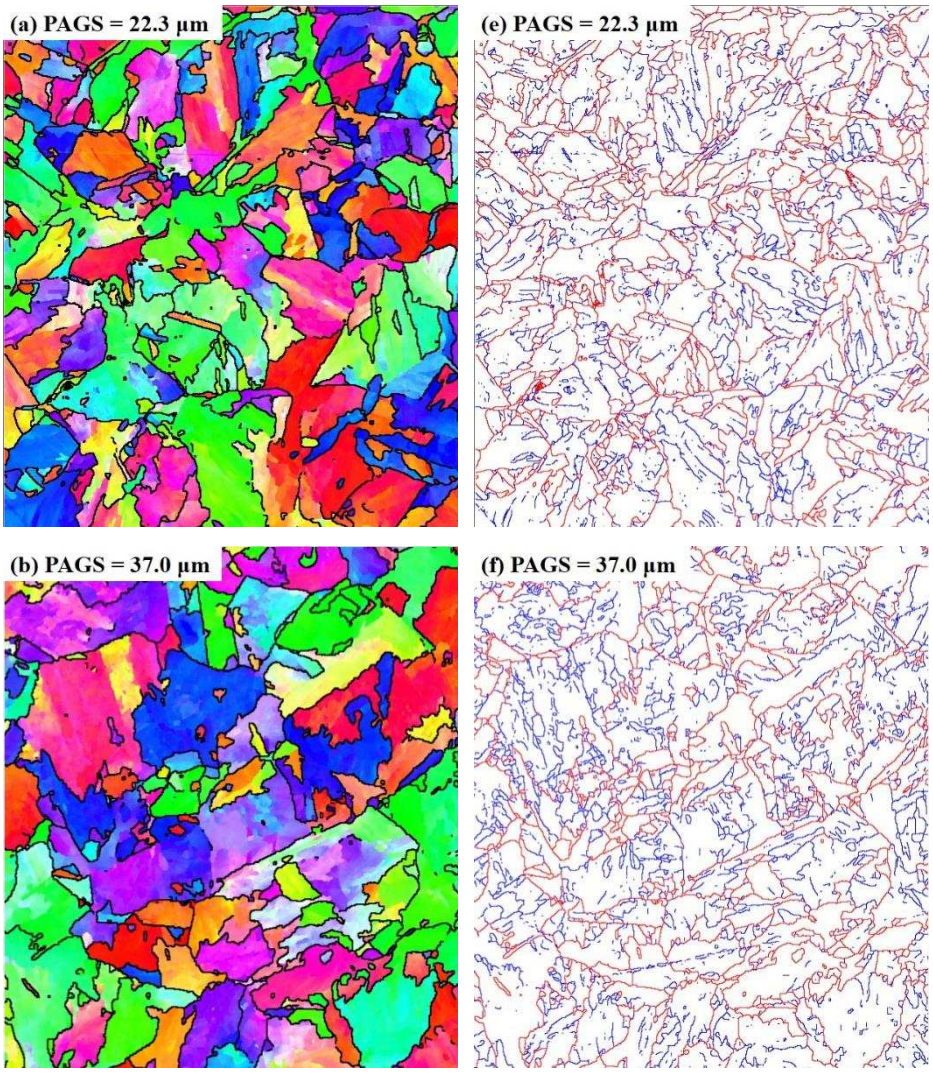

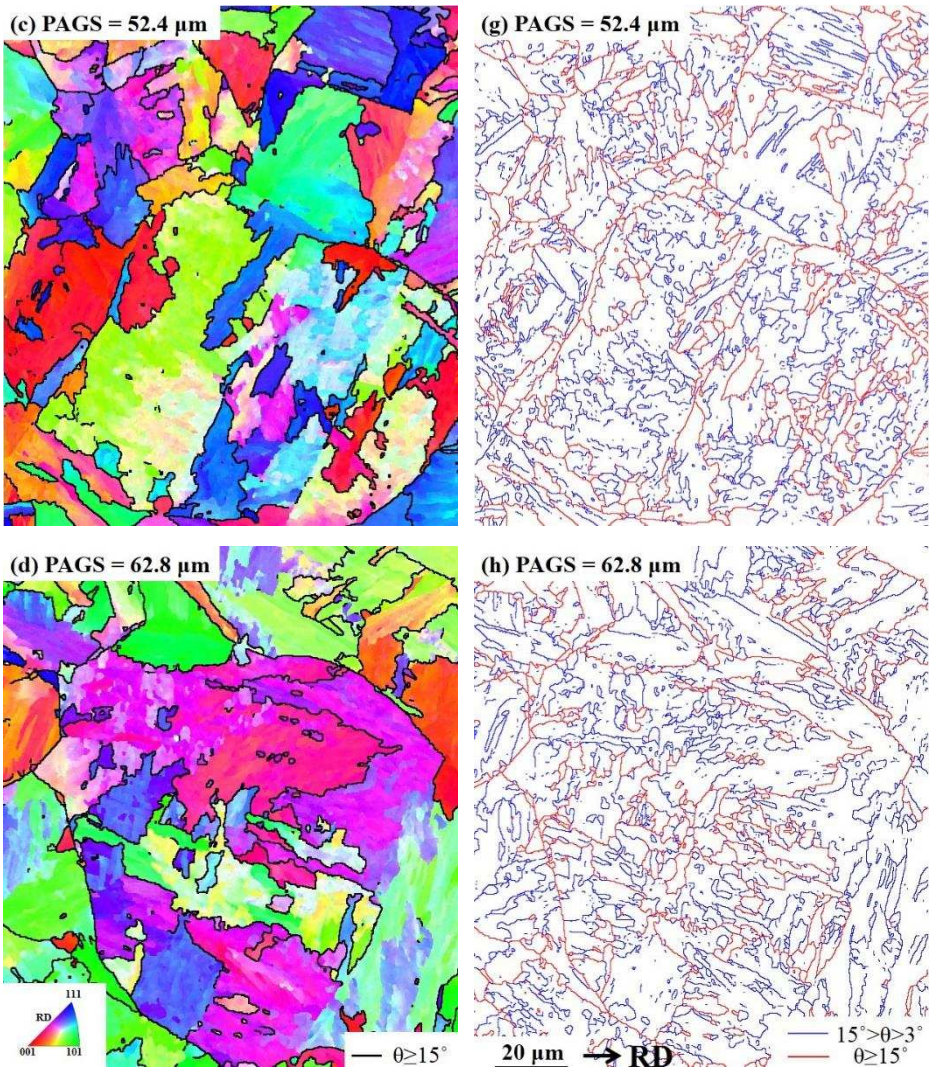

Figure 5 EBSD maps of the microstructures transformed from fully recrystallised austenite with different PAGSs: (a)~(d) inverse pole figure coloured orientation image maps corresponding to microstructures with PAGS of 22.3 *μm, 37.0 μm, 52.4 μm and* 62.8 *μm, respectively, where black lines represent high angle boundaries with* disorientation greater than 15°; (e)~(h) boundary maps corresponding to the same area in (a)~(d) respectively, where blue lines represent low angle boundaries with disorientation between 3° and 15° whilst red lines represent high angle boundaries with disorientation greater than 15°.

The increase in the HAGB density results in refined microstructure. To quantify

the microstructure refinement, disorientation angle threshold values should be selected. Different disorientation angle threshold values have been used to define microstructure parameters that can be related to certain mechanical properties, and the microstructural unit size that controls strength may differ from that controls toughness. Disorientation angle threshold values of 4° and 15° are typical threshold values to define the microstructural unit sizes for strengthening and toughening, respectively [17, 18]. Low disorientation angle (4°) grain size is one of the factors that controls the yield and tensile strength of steel because boundaries with disorientation angles above this value are expected to be able to oppose dislocation movements, while high angle grain boundaries ($\theta \geq 15°$) provide effective barriers to cleavage fracture [17, 19]. The grain size measured against the high disorientation angle (15°) is usually called the effective grain size.

The grain size defined by different disorientation threshold values, 4° and 15°, are measured by a linear intercept method in the Channel 5 software respectively. The geometric means of the linear intercept lengths in both horizontal and vertical directions were calculated as in reference [20] and are shown in Figure 6.

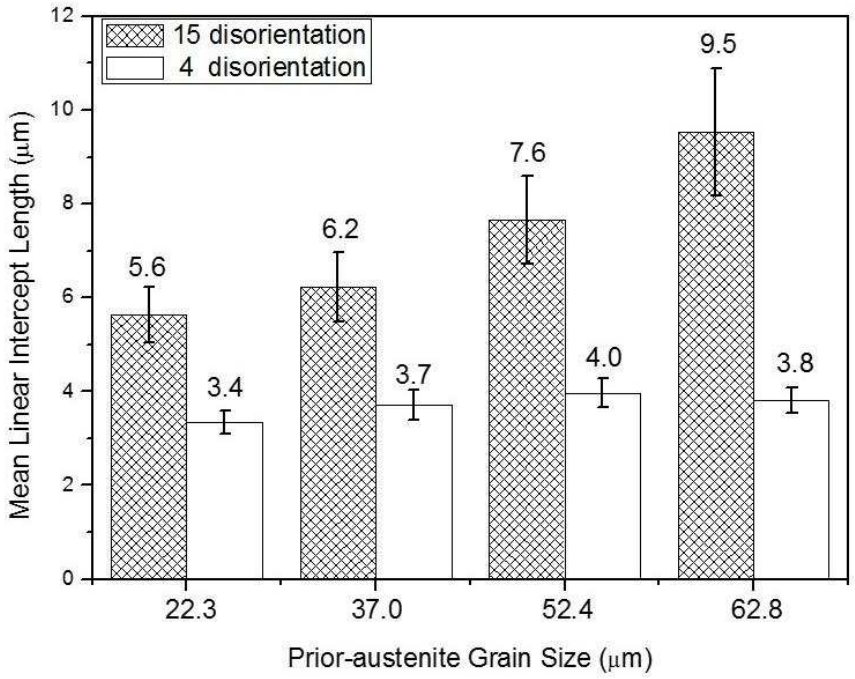

Figure 6 Microstructure size parameter measured against two disorientation criteria, 4˚ and 15˚, as geometric mean of the linear interception lengths in horizontal and vertical direction from the EBSD maps measured of the continuously cooled microstructures with different PAGSs. Error bars represent 95% confidence levels of the measurement.

In Figure 6, we can see clearly that the effective grain size decreases gradually with the reduction of PAGS from 62.8 μm to 22.3 μm, while the mean intercept lengths against 4˚ of these four microstructures are very similar. These results suggested that for BF microstructures transformed from fully recrystallised austenite, reducing the PAGS can effectively refine the transformed microstructure.

4. Discussion

Without austenite deformation, the continuously cooled microstructures with different PAGSs, varying from 22.3 μm to 62.8 μm, mainly consist of BF laths. As can be seen from Figure 4 and Figure 6 that altering the PAGS, both the morphology and the effective grain size of the transformed BF microstructure are changed.

Due to the BF transformation having displacive transformation characteristics, the BF transformation cannot cross austenite grain boundaries and the BF laths and their parent austenite grains are crystallographically related by a certain orientation relationship (OR) within the Bain region [2]. Owing to this OR and the symmetry of austenite, there are 24 possible BF orientation variants for each austenite grain and these variants can form a special pattern in pole figures which can be used to identify each parent austenite grain. During BF transformation, some or all of the variants can form in an austenite grain and the selection of variants during transformation will have a profound influence on the morphology and grain refinement of the final microstructure. Therefore, to further investigate the differences in BF morphology and grain refinement from a crystallographic perspective, a comparison is made between the BF microstructures with PAGSs of 37.0 μm (small) and 62.8 μm (large) and a prior-austenite grain was identified in each EBSD maps of these two BF microstructures. The {100} pole figures of the BF orientations of these two prior-austenite grains are shown in Figure 7 (a), (c) and the IPF coloured orientation maps of them are illustrated in Figure 8 (a), (d) respectively.

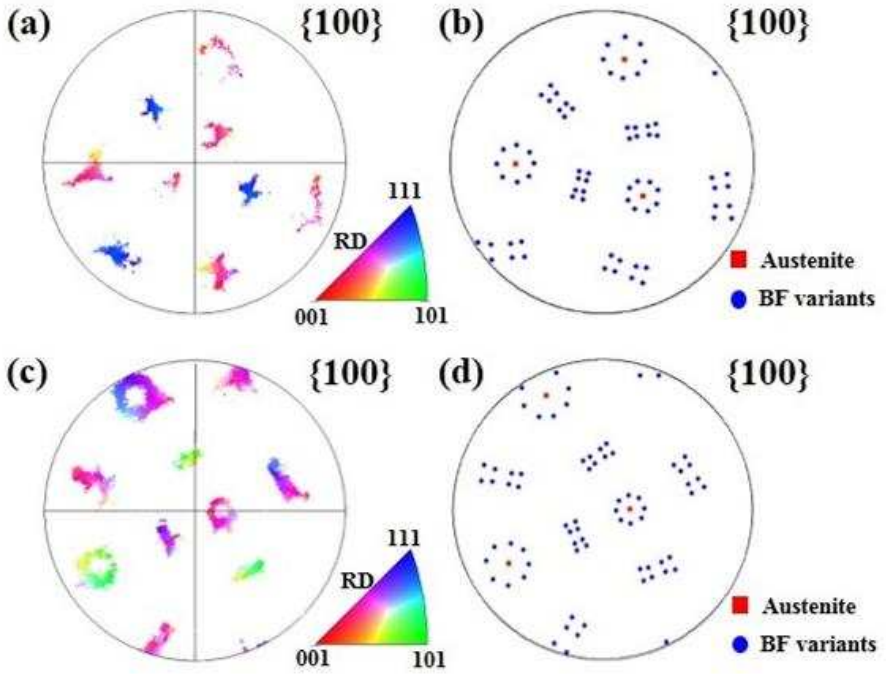

Figure 7 {100} pole figures of the BF orientation in single parent austenite grains with (a) small (37.0 *μm) and (c) large (62.8 μm) PAGS; {100} pole figures of the* calculated austenite orientations and corresponding ferrite orientation variants with (b) small and (d) large PAGS.

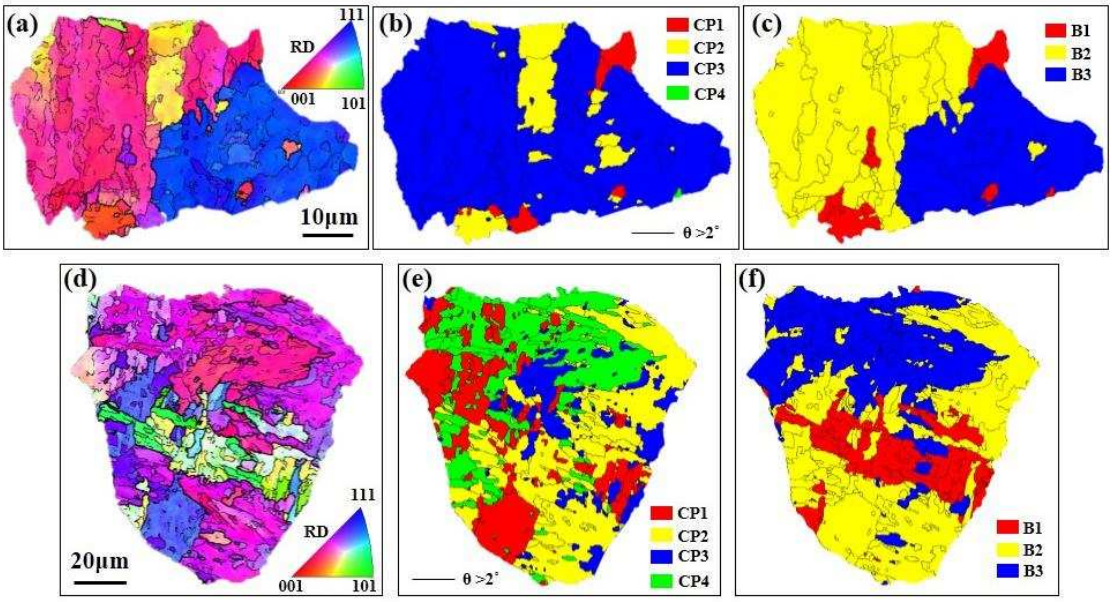

Figure 8 IPF coloured orientation maps (a) and (d), close-packed plane group maps

(b) and (e) and Bain group maps (c) and (f) for BF microstructures in single parent austenite grains with the small (37.0 *μm) and large (62.8 μm) PAGS respectively.*

Since the Kurdjumov–Sachs (K–S) orientation relationship ($\{111\}_\gamma//\{110\}_\alpha$, $<110>_\gamma//<111>_\alpha$) generally provides good predictions for the BF transformation in steels [21], it was adopted as the OR in this research, although the OR should be irrational as predicted by the phenomenological theory [22]. The method proposed by Tari et al. [23] was used to evaluate the orientations of these two parent austenite grains, and the results were used to calculate the 24 K-S variants of each austenite grain. These results are shown in Figure 7 (b), (d) respectively, and good matches can be found between the pole figures of the experimentally determined BF orientations and calculated ferrite orientation variants. The 24 K-S variants calculated can be divided into four close-packed plane (CP) groups, each of which consists of six variants sharing the same parallel relationship of close-packed planes with austenite. K–S variants can also be discriminated into three Bain groups according to three distinctive variants of the Bain correspondence [24]. The sequence of the 24 K-S variants and their corresponding CP and Bain groups for this investigation was adopted from Takayama et al. [25]. To reveal detailed crystallographic features, the colours in the orientation maps were changed to show different colours for different CP and Bain groups. These maps are termed as CP and Bain group maps and are shown in Figure 8 (b), (e) and Figure 8 (c), (f) for the two BF microstructures with different PAGSs, respectively.

For the BF microstructure with the small PAGS (37.0 μm), Figure 8 (a), parallel BF laths can be clearly revealed by low angle grain boundaries. It is also evident from Figure 7 (a), (b) that an intense variant selection occurred, and only a small fraction of the 24 K-S variants formed. Furthermore, the entire austenite grain is dominated by a single CP group with blue colour as shown in the CP map, Figure 8 (b), but consists of two Bain groups, yellow and blue, as shown in the Bain group map, Figure 8 (c).

For the BF microstructure with the large PAGS (62.8 μm) shown in Figure 8(d), a more complicated BF microstructure was formed, and nearly all the 24 K-S variants exist, Figure 7 (c), (d). From the CP group map shown in Figure 8 (e), it is evident that the entire austenite grain is occupied by intersecting CP groups, signifying variants from the same CP groups are no longer preferentially formed side by side. Interestingly, although adjacent laths come from different CP groups, they mainly belong to the same Bain group as shown in the Bain group map in Figure 8 (f), except in the central part of the parent austenite grain where different Bain groups intersect.

4.1 Effect of PAGS on variant selection

The above analysis clearly shows that there is a limited number of BF orientation variants formed in the smaller austenite grain. This suggests that after nucleation on the most potent austenite grain boundaries, the BF laths rapidly develop across the whole parent grain before nucleation sites on other austenite grain boundaries become potent enough. However, for the larger austenite grain, and because of the larger intercept length and higher volume, before the initially nucleated BF laths expand across the complete austenite grain, other austenite grain boundaries become potent

enough, and there is still enough volume of austenite left for the development of these nuclei. Since variant selection happens during the BF nucleation on austenite grain boundaries through the reduction of the BF/austenite boundary energy and other mechanisms [26], the variants selected on the austenite grain boundaries varies with the austenite grain boundary characteristics. Therefore, in austenite grains with a large PAGS, BF laths of different variant types can develop, and the variant selection is less intense than that observed in the small-grained austenite. This is consistent with previous research [27, 28], where austenite grains with a small PAGS transformed into limited types of variants compared with large-grained austenite. Additionally, it was found in research [28] that the size of BF blocks which consisted of variants with a similar orientation, was nearly equal to the linear intercept length of the parent austenite when the size of parent austenite was smaller than ~30 μm. In austenite with a grain size higher than this value, the block size was found to be considerably smaller than the size of the austenite grain, indicating that more blocks and thus more variants will be formed in coarse-grained austenite.

4.2 Effect of PAGS on grain refinement

Due to the difference in variant selection as shown in Figure 7, the chance of forming HAGBs within each austenite grain is lower for the small-grained austenite compared to the large-grained austenite. This characteristic is also illustrated in the Bain group maps in Figure 8 (c) and (f) because in the same austenite grain, the disorientation angles of boundaries between two variants belonging to different Bain groups are higher than 20.6° for the K-S OR. However, with the reduction of PAGS

from 62.8 μm to 22.3μm, the effective grain size gradually decreases from 9.5 μm to 5.6 μm, indicating the density of HAGB is higher in the transformed microstructure with a smaller PAGS. This discrepancy can be understood by analysing the densities and fractions of HAGBs with different disorientation angles shown in Figure 9.

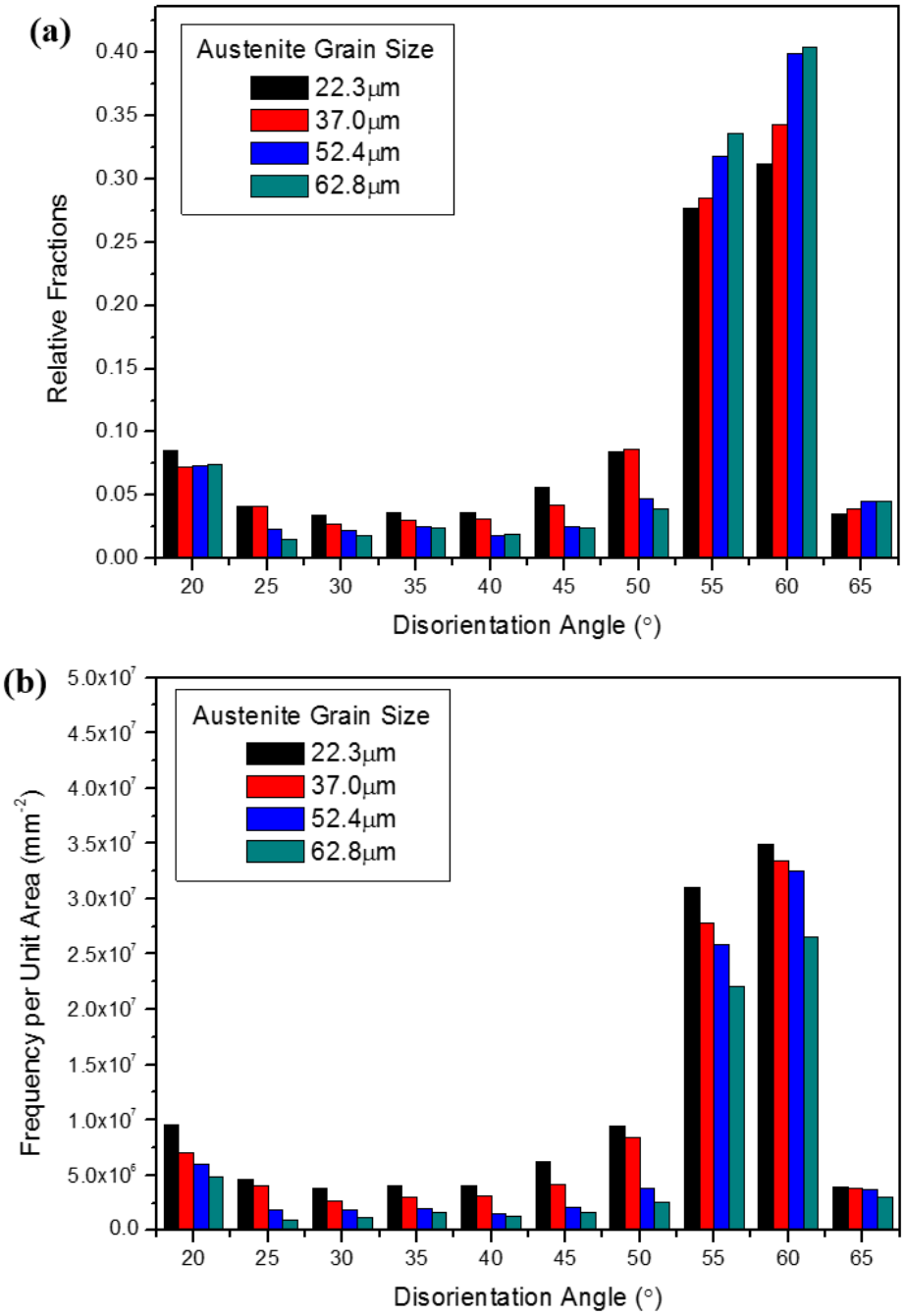

Figure 9 Histograms showing (a) the relative fractions of boundaries and (b) the boundary densities in terms of absolute number per unit area with different

disorientation angles from 15º to 62.8º.

Based on the disorientation angles between 24 K-S variants, HAGBs with different disorientation angles are formed by different mechanisms. The whole disorientation angle scope of HAGB can be divided into three ranges, range 1 ($15^\circ \leq \theta < 21^\circ$), range 2 ($21^\circ \leq \theta < 47^\circ$) and range 3 ($47^\circ \leq \theta \leq 62.8^\circ$).

HAGBs with disorientations angles within the range 1 are mainly the boundaries between variants transformed in the same austenite grain and belonging to the same Bain group. HAGBs with disorientations angles within the range 2 are the boundaries between variants transformed from different austenite grains and contacted with each other near the PAGBs. HAGBs with disorientations angles within the range 3 are mainly the boundaries between variants transformed in the same austenite grain but belonging to different Bain groups.

In Figure 9(a), we can see that with the decrease of PAGS, the fractions of HAGBs with disorientation angles within the range 2 are increased, while the fractions of HAGBs with disorientation angles within the range 3 are reduced. No great changes are found in the fractions of HAGBs with disorientation angles within the range 1. These results indicate that the chance of forming HAGBs within each austenite grain is lower for the small-grained austenite compared to the large-grained austenite and for the small-grained austenite more fractions of HAGBs are formed at the PAGBs, leading to the increased fraction of HAGBs within the range 2 as the PAGS is reduced. But, with the reduction of PAGS, the quantity of prior-austenite

grains and thus the total area of PAGBs per unit volume is increased, leading to the increased absolute densities of HAGBs within all the disorientation angle ranges as shown in Figure 9(b).

Furthermore, besides the range 2, the disorientation angles of boundaries between variants transformed from different austenite grains can also fall into other disorientation angle ranges, 1 and 3. With the increase of the total PAGB area per unit volume as the PAGS is reduced, the influence of PAGB on boundary densities within the ranges 1 and 3 will be more and more evident.

Therefore, although intense variant selections exist in transformed microstructures with small PAGSs, due to the large austenite grain quantity and thus the large total PAGB area per unit volume of the small-grained austenite, the transformed microstructure is refined with the reduction of PAGS.

4.3 Effect of PAGS on the arrangement of CP and Bain groups

Besides variant selection, the arrangements of CP and Bain groups are also quite different between small-grained and large-grained austenite. During the bainite transformation, the parent austenite grain is usually divided into packets, each of which consists of a group of laths with nearly the same trace direction on a polished surface due to their habit planes being in close proximity to each other. Since the variants belonging to the same CP group have the closest habit planes [26], packets usually consist of variants coming from the same CP group. In other words, BF laths belonging to the same CP group are usually formed side by side. However, this is only

the case in austenite with a small PAGS as shown in Figure 3 (b) and Figure 8 (b). For the austenite with a large PAGS, the parent austenite grains cannot be clearly divided into packets as shown in Figure 3 (d) and the BF laths belonging to different CP groups are formed adjacently and are well-intersected, Figure 8 (e). In this case, austenite grains are more conveniently described as being divided by Bain groups instead of CP groups. This is consistent with previous research [25] that the variants belonging to the same Bain group are created adjacently in bainite transformed at higher temperatures and thus smaller driving forces.

Obviously, it is these differences in the arrangement of CP groups between austenite grains with small and large PAGS that result in the differences in optical morphology. For transformed microstructure with the small PAGS, a single CP group is dominant, and the boundaries between parallel laths are quite continuous, Figure 8 (a), and thus can be identified easily in optical micrographs or SEM micrographs. However, in transformed microstructure with the large PAGS, the BF laths belonging to different CP groups were observed to be adjacent to each other, thus forming an interlocking morphology. Due to the incomplete transformation phenomenon of bainite [2] and this intricate morphology of BF laths, equiaxed carbon-rich M/A particles are found between the BF laths. Furthermore, the lath boundaries are less continuous as shown in the upper part of Figure 8(a), and are therefore not obvious from optical micrographs. Although it is possible to say that it is the impingement between different Bain groups that results in this interlocking morphology, it also exists in the area where a single Bain group is dominant, as shown in the upper part of

austenite grain in Figure 8 (c). This latter situation is consistent with the results in previous research [29], where adjacent non-parallel sets of BF laths were found belonging to the same Bain group and appearing as a single grain in the optical micrographs. Although the thickening of BF laths during continuous cooling usually covers up this interlocking morphology in optical micrographs, it can be clearly revealed in partially transformed microstructures [29-31].

The possible formation mechanism of a variant pair belonging to a different CP group but the same Bain group maybe can be explained from the variant selection during the BF nucleation on lattice defects. Since in this research, the continuous cooling rate is relatively slow, the BF transformation happens at a relatively high temperature. Therefore, the transformation strain is accommodated plastically by the austenite and BF, and thus dislocations could be introduced into the austenite which have characteristics that are strongly related to the first nucleated variant [2]. And according to the variant selection model proposed by Butron-Guillen et al. [21], the formation of each variant can be closely linked to a particular slip system. Therefore, it is possible that the dislocations in the austenite introduced by the first nucleated variant is a suitable nucleation site for the sympathetic nucleation of other BF laths, defined as strain-induced nucleation [2], and indeed a two stage nucleation behaviour has been observed before [30]. The first stage is associated with the primary plates nucleating at the austenite boundaries and grows towards the inside of austenite grains. The second stage is the secondary plates nucleating on the primary plates and growing in a different direction [30]. Lambert-Perlade et al. [21] suggested this particular kind

of variant pairs becomes favoured because that this particular spatial and crystallographic kind of variant pair is able to reduce the plastic deformation in the austenite phase, which could help the growth of BF laths. A separate investigation by Takayama et al.[25] proposed that the reduction in boundary energies between variants is the reason for the formation of this particular variant pair because variants belonging to the same Bain group usually have smaller disorientation angles and that the boundary energy decreases significantly with decreasing disorientation angle below about 15˚.

Interestingly, this variant pairing mechanism is not dominant in the BF microstructures with the small PAGS. Although the austenite grain size exhibits an effect on the bainite start temperature and transformation kinetics, the possibility of transformation temperature acting as the dominant factor can be excluded. This is due to the fact that the same differences resulted from PAGS were also observed in isothermally transformed bainite microstructures [30], although no explanation was provided.

A review of the martensite transformation shows that there is a very similar nucleation process to what this research has found in large-grained austenite. This process is known as autocatalysis, which describes the situation where plates of martensite form and induce new embryos that are then available for further transformation [2]. Autocatalysis is responsible for the bursts of transformation that the initial formation of a plate stimulates a disproportionately large degree of further transformation and most importantly, it was found that the burst temperature of

martensite is decreased with the reduction of austenite grain size [32, 33]. This effect of austenite grain size is attributed to the fact that the burst of martensite transformation arises as a consequence of the severe elastic and plastic disturbance of the austenite in the immediate vicinity of a plate of martensite [2]. It is the displacive transformation strain that causes this disturbance. The intensity of the stress and strain field set-up by a plate is proportional to its size, which, in the case of the firstly formed plates, can be considered to be limited by the grain size of the austenite. It follows that the formation of one plate in a coarser austenite grain will cause a higher range of elastic and plastic disturbance, and thus a higher burst temperature [32]. However, the situation is different in the BF transformation, where laths are stopped below a certain size due to the plastic accommodation of the transformation strain in the austenite, and the formation of laths actually lowers the average transformation strain volume from around 0.23 to 0.13 [2]. Therefore, the elastic and plastic disturbance of the austenite should not be significantly influenced by the size difference of laths and thus PAGS.

A more reasonable explanation could be based on the driving force of BF transformation from austenite near the BF/austenite interface. Because of the fact that the post-transformation carbon content of BF tends to be significantly higher than equilibrium and the diffusion coefficient of carbon in austenite is significantly lower than that in ferrite, there are carbon enriched regions in the austenite around the existing BF laths [34]. Since the grain boundary area per unit volume is lower in the large-grained austenite, fewer BF laths form per unit volume at a certain time than

those in the small-grained austenite, as schematically shown in Figure 10. Furthermore, BF grows under a relatively small driving force, which is only adequate for the development of a low carbon nucleus [2]. Therefore, the carbon concentration of the austenite near the existing BF laths can be reduced sufficiently in large-grained austenite to a level that strain-induced nucleation sites become potent enough to generate BF, whereas in small-grained austenite the carbon diffusion fields of adjacent BF laths are more likely to overlap, keeping the carbon concentration higher than the level to allow nucleation sites to be potent enough. The low cooling rate in the present research also provides enough time at high temperatures, which facilitate the carbon diffusion in austenite. However, more details on the transformation strain plastic accommodation and carbon distribution profile are needed to propose a clear answer.

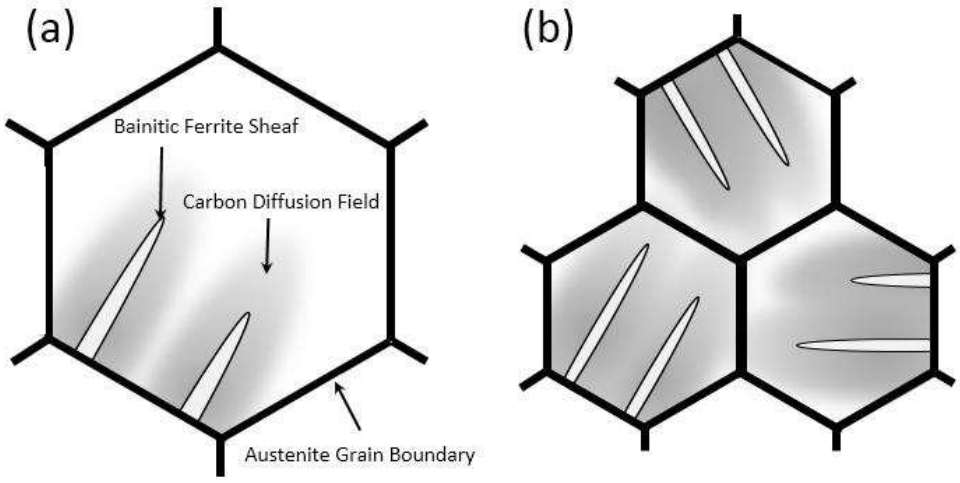

Figure 10 Schematic illustration of the difference in carbon diffusion fields in the austenite with (a) large and (b) small PAGS.

5. Conclusions

In this research specimens with various austenite grain sizes were processed to investigate the effect of PAGS before continuous cooling on the microstructural evolution and grain refinement. Through detailed crystallographic analysis, it has been found that:

(1) Under a relatively slow continuously cooling rate, intense BF variant selection occurs for small-grained austenite and BF laths, belonging to the same CP group, tend to grow side by side forming packet structures that are visible in optical micrographs.

(2) For large-grained austenite, nearly all the variants are formed and variants from different CP groups but the same Bain group tend to grow together forming an interlocking structure, which is difficult to distinguish in optical micrographs. This morphology difference may be attributed to possible lower carbon concentrations near the BF and austenite interfaces in the large-grained austenite than those in the small-grained austenite.

(3) Although intense variant selections exist in transformed microstructures with small PAGSs, due to the large austenite grain quantity and thus the large total PAGB area per unit volume of the small-grained austenite, the transformed microstructure is refined with the reduction of PAGS.

Acknowledgements

The authors would like to thank both Companhia Brasileira de Metalurgia e

Mineração (CBMM) and the China Scholarship Council (CSC) for their financial support of this research programme.

References

1. J.-Y. Yoo et al., “New development of high grade X80 to X120 pipeline steels,” Materials and Manufacturing Processes, 26 (2011) 154-160.

2. H.K.D.H. Bhadeshia, Bainite in steels (London, The Institute of Materials, 2001).

3. J. Barford and W. Owen, “The effect of austenite grain size and temperature on the rate of bainita transformation,” Metal Science and Heat Treatment, 4 (1962) 359-360.

4. M. Umemoto et al., “Transformation kinetics of bainite during isothermal holding and continuous cooling,” Tetsu-to-Hagane, 68 (1982) 461-470.

5. S.-J. Lee et al., “Effect of austenite grain size on the transformation kinetics of upper and lower bainite in a low-alloy steel,” Scripta Materialia, 59 (2008) 87-90.

6. G. Rees and H. Bhadeshia, “Bainite transformation kinetics Part 1 Modified model,” Materials Science and Technology, 8 (1992) 985-993.

7. E. Davenport et al., “Influence of Austenite Grain Size upon Isothermal Transformation Behavior of SAE 4140 Steel,” Trans. AIME, 145 (1941) 301.

8. L. Graham and H. Axon, Iron and Steel Inst, 191 (1959) 361-368.

9. G. Xu et al., “A new approach to quantitative analysis of bainitic transformation in a superbainite steel,” Scripta Materialia, 68 (2013) 833-836.

10. A. Matsuzaki and H. Bhadeshia, “Effect of austenite grain size and bainite morphology on overall kinetics of bainite transformation in steels,” Materials Science and Technology, 15 (1999) 518-522.

11. S. Kang et al., “Prediction of Bainite Start Temperature in Alloy Steels with Different Grain Sizes,” ISIJ international, 54 (2014) 997-999.

12. K. Hulka and J. Gray, “High Temperature Processing of Line Pipe Steels,” Proceedings of the International Symposium Niobium, 2001, 587-612.

13. C. Heckmann et al., “Development of low carbon Nb–Ti–B microalloyed steels for high strength large diameter linepipe,” Ironmaking & steelmaking, 32 (2005) 337-341.

14. G.F. Vander Voort, Metallography, principles and practice (ASM International,

1984).

15. D. Jorge-Badiola et al., “Influence of Thermomechanical Processing on the Austenite-Pearlite Transformation in High Carbon Vanadium Microalloyed Steels,” Isij International, 50 (2010) 546-555.

16. S. Hashimoto and M. Nakamura, “Effects of microalloying elements on mechanical properties of reinforcing bars,” Isij International, 46 (2006) 1510-1515.

17. H. Kitahara et al., “Crystallographic features of lath martensite in low-carbon steel,” Acta Materialia, 54 (2006) 1279-1288.

18. W. Wang et al., “Relation among rolling parameters, microstructures and mechanical properties in an acicular ferrite pipeline steel,” Materials & Design, 30 (2009) 3436-3443.

19. S. Kim et al., “Relationship between yield ratio and the material constants of the Swift equation,” Metals and Materials International, 12 (2006) 131-135.

20. L. Sun et al., “Mapping microstructure inhomogeneity using electron backscatter diffraction in 316L stainless steel subjected to hot plane strain compression tests,” Materials Science and Technology, 26 (2010) 1477-1486.

21. M. Butrón-Guillén et al., “A variant selection model for predicting the transformation texture of deformed austenite,” Metallurgical and Materials Transactions A, 28 (1997) 1755-1768.

22. P.M. Kelly, “Crystallography of lath martensite in steels,” Materials Transactions, 33 (1992) 235-242.

23. V. Tari et al., “Back calculation of parent austenite orientation using a clustering approach,” Journal of Applied Crystallography, 46 (2013) 210-215.

24. A.-F. Gourgues, “Microtexture induced by the bainitic transformation in steels during welding. Effect on the resistance to cleavage cracking,” Materials Science Forum, 426 (2003) 3629-3634.

25. N. Takayama et al., “Effects of transformation temperature on variant pairing of bainitic ferrite in low carbon steel,” Acta Materialia, 60 (2012) 2387-2396.

26. T. Furuhara et al., “Key factors in grain refinement of martensite and bainite,” Materials Science Forum, 638 (2010) 3044-3049.

27. V. Pancholi et al., “Self-accommodation in the bainitic microstructure of ultra-high-strength steel,” Acta Materialia, 56 (2008) 2037-2050.

28. L. Rancel et al., “Measurement of bainite packet size and its influence on cleavage fracture in a medium carbon bainitic steel,” Materials Science and Engineering: A, 530 (2011) 21-27.

29. A. Lambert-Perlade et al., “Austenite to bainite phase transformation in the

heat-affected zone of a high strength low alloy steel," Acta Materialia, 52 (2004) 2337-2348.

30. L. Lan et al., "Effect of austenite grain size on isothermal bainite transformation in low carbon microalloyed steel," Materials Science and Technology, 27 (2011) 1657-1663.

31. D. Tian et al., "Correlation between microstructural features of granular bainite, roughness of fracture surface and toughness of simulated CGHAZ in QT type HSLA steels," Scandinavian Journal of Metallurgy, 25 (1996) 87-94.

32. J. Guimarães and J. Gomes, "A metallographic study of the influence of the austenite grain size on martensite kinetics," Acta Metallurgica, 26 (1978) 1591-1596.

33. M. Umemoto and W. Owen, "Effects of austenitizing temperature and austenite grain size on the formation of athermal martensite in an iron-nickel and an iron-nickel-carbon alloy," Metallurgical transactions, 5 (1974) 2041-2046.

34. S. Mujahid and H. Bhadeshia, "Partitioning of carbon from supersaturated ferrite plates," Acta metallurgica et materialia, 40 (1992) 389-396.